

Constraining the star formation histories of spiral bulges

R. N. Proctor,¹ A. E. Sansom¹ and I. N. Reid²

¹Centre for Astrophysics, University of Central Lancashire, Preston PR1 2HE

²California Institute of Technology, 105-24, Pasadena, CA 91126, USA

Accepted 1999 July 27. Received 1999 July 22; in original form 1999 March 22

ABSTRACT

Stellar populations in spiral bulges are investigated using the Lick system of spectral indices. Long-slit spectroscopic observations of line strengths and kinematics made along the minor axes of four spiral bulges are reported. Comparisons are made between central line strengths in spiral bulges and those in other morphological types [elliptical, spheroidal (Sph) and S0]. The bulges investigated are found to have central line strengths comparable to those of single stellar populations of approximately solar abundance or above. Negative radial gradients are observed in line strengths, similar to those exhibited by elliptical galaxies. The bulge data are also consistent with correlations between Mg_2 , Mg_2 gradient and central velocity dispersion observed in elliptical galaxies. In contrast to elliptical galaxies, central line strengths lie within the loci defining the range of $\langle Fe \rangle$ and Mg_2 achieved by Worthey's solar abundance ratio, single stellar populations (SSPs). The implication of solar abundance ratios indicates significant differences in the star formation histories of spiral bulges and elliptical galaxies. A 'single zone with infall' model of galactic chemical evolution, using Worthey's SSPs, is used to constrain the possible star formation histories of our sample. We show that the $\langle Fe \rangle$, Mg_2 and $H\beta$ line strengths observed in these bulges cannot be reproduced using primordial collapse models of formation but *can* be reproduced by models with extended infall of gas and star formation (2–17 Gyr) in the region modelled. One galaxy (NGC 5689) shows a central population with a luminosity-weighted average age of ~ 5 Gyr, supporting the idea of extended star formation. Kinematic substructure, possibly associated with a central spike in metallicity, is observed at the centre of the Sa galaxy NGC 3623.

Key words: galaxies: abundances – galaxies: evolution – galaxies: formation – galaxies: spiral – galaxies: stellar content.

1 INTRODUCTION

The recently developed Lick system of spectral indices (Faber et al. 1985; Worthey et al. 1994) has provided powerful tools for the investigation of composite populations. Diagnostic plots, such as $\langle Fe \rangle$ versus $H\beta$ and Mg_2 versus $\langle Fe \rangle$, (where $\langle Fe \rangle$ is the average of Fe5270 and Fe5335 indices) break the age/metallicity degeneracy and have illustrated characteristics and trends in elliptical galaxies that constrain their possible star formation histories (SFHs). This paper compares the line strengths in four spiral bulges with those observed in other morphologies and places constraints on possible SFHs in the sample. Comparison of the SFHs of spiral bulges to that of elliptical galaxies is informative as the two morphologies show numerous similarities. Bulges exhibit similar surface brightness profiles and kinematic structures to ellipticals, and form an overlapping continuation of the elliptical locus in the Fundamental Plane (Bender, Burstein & Faber 1993). Colours and colour gradients in the two types of spheroid are also similar (Balcells & Peletier 1994). However,

despite similarities in physical and photometric properties, the two galaxy types are found in very different environments, with the majority of ellipticals located in clusters, while spiral galaxies are preferentially found in the field. Another important factor in the environment of spiral bulges is the presence of the disc, which severely limits possible merger histories.

Observations of elliptical galaxies have shown them to possess high central line strengths. Gradients are observed in metallicity-sensitive features, indicative of dissipation in the formation process. The $H\beta$ index shows no indication of systematic gradients in age (Carollo, Danziger & Buson 1993; Davies, Sadler & Peletier 1993; Fisher, Franx & Illingworth 1996; Gorgas et al. 1997; Vazdekis et al. 1997). Modelling of Lick indices in elliptical galaxies, for comparison to observation, has been carried out by a number of authors (Worthey, Dorman & Jones 1996; Greggio 1997; Vazdekis et al. 1997; Sansom & Proctor 1998). These studies have shown that the high line strengths found at the centre of elliptical galaxies can only be achieved if the bulk of the observed population forms from pre-enriched gas. Two possible

processes have been proposed to produce this pre-enrichment. One possibility is an initial mass function (IMF) biased towards high-mass stars in the early stages of galaxy formation. In this scenario the first few generations of stars generate large quantities of metals (Gibson & Matteucci 1997; Vazdekis et al. 1997). Alternatively, a period of star formation (SF), and thus interstellar medium (ISM) enrichment, with a Salpeter IMF prior to the main burst can produce the necessary pre-enrichment. This delayed burst of star formation may correspond to a merger/interaction model of elliptical galaxy formation (Sansom & Proctor 1998).

The second important feature of line strengths in ellipticals is their high central Mg_2 with respect to $\langle Fe \rangle$ when compared with models assuming solar abundance ratios (Worthey, Faber & González 1992; Davies et al. 1993; Gorgas et al. 1997; Greggio 1997). This Mg_2 excess is interpreted as indicating $[Mg/Fe]$ greater than solar (Davies et al. 1993). High $[Mg/Fe]$ ratios can be achieved by star formation times of $\lesssim 1$ Gyr, in accordance with the short time-scales of gas inflow in both merger/interaction (Barnes & Hernquist 1996) and primordial collapse models of elliptical galaxy formation (Theis, Burkert & Hensler, 1992). Short bursts of star formation ensure that the metal enrichment of the ISM, from which the bulk of the population forms, is mainly produced in the Type II supernovae that are the main sites for production of Mg. The biased IMF proposal also naturally produces an excess of Type II supernovae (and consequently Mg_2) due to an overproduction of high-mass stars. While both merger and primordial collapse (with biased IMF) models can successfully reproduce the indices in the Mg_2 versus $\langle Fe \rangle$ plane, the high central $H\beta$ values of many elliptical galaxies are a challenge to primordial collapse models. In contrast, merger models clearly predict the existence of younger populations in these objects.

Observations of other galaxy morphologies, such as S0s (Sil'chenko 1993; Fisher et al. 1996) and Sphs (Gorgas et al. 1997), show differences between central line strengths in various galaxy types in the $\langle Fe \rangle$ versus Mg_2 plane. S0s tend to exhibit weaker Mg_2 lines for a given $\langle Fe \rangle$ than do Es while still showing an excess with respect to values for solar abundance ratio SSPs. Gorgas et al. (1997) showed that Sphs approximately follow solar abundance ratio SSP loci in the $\langle Fe \rangle$ versus Mg_2 diagnostic plot. Low-luminosity spiral bulges observed by Jablonka, Martin & Arimoto (1996) also span the region of the Mg_2 versus $\langle Fe \rangle$ plot occupied by Worthey's solar abundance ratio SSPs (Worthey 1998), while some high-luminosity bulges in their sample exhibit greater than solar $[Mg/Fe]$.

Observations of individual stars in the bulge of our own Galaxy, while hampered by obscuration, have provided interesting insights into the population present. Minniti et al. (1995) report a broad range of metallicities ($-2 < [Fe/H] < +1$) in K giants in the Galactic bulge and indicate the presence of a metallicity gradient.

Observations of resolved M giants in the centre of the bulge of our own Galaxy indicate approximately solar abundances and also indicate a gradient in metallicity (Frogel 1998). Recent episodes of star formation at the centre of the bulge, with several bursts having occurred over the past few 100 Myr, have also been suggested (Blum, Sellgren & Depoy 1996; Frogel 1998). These observations suggest that the population of the bulge of our own Galaxy has a complex and extended SFH.

Our long-slit observations of spiral bulges allow comparison of central line strengths and gradients to those in other galaxy types and constrain possible SFH in the bulges. We probe whether the similarities between bulges and elliptical galaxies in morphological and photometric properties are the result of similar formation processes or are rather the result of the evolution of differing histories to similar present-day forms. In Section 2 the observations, data reduction and error estimates are outlined. Results of our analysis and comparison with other Hubble types are reported in Section 3. Comparison to models are detailed in Section 4. Our conclusions and the direction of future work are outlined in Section 5.

2 OBSERVATIONS AND DATA REDUCTIONS

2.1 Observations

Using the Palomar 5.08-m telescope on 1995 March 31, long-slit spectroscopy was carried out along the minor axes of the bulges of four, approximately edge-on, spiral galaxies (Table 1 and Fig. 1). We chose to observe edge-on systems along their minor axes as disc obscuration of bulge light is thus concentrated on one side of the bulge. A fifth galaxy (NGC 4013) was also observed but appeared to have a bright foreground star slightly offset from the centre of the galaxy. Consequently, this galaxy was excluded from data reductions. The Double Spectrograph was used (Oke & Gunn 1982) with a 5700-Å dichroic filter and Texas Instruments CCDs on both red and blue arms. Wavelength coverage in the blue was 4560–5430 Å at a resolution of 1.1 Å per pixel. In the near infrared the range 8235–8860 Å was observed at a resolution of 0.8 Å per pixel. The blue wavelength range was chosen to include the $H\beta$, Mg and Fe absorption features calibrated by Faber et al. (1985) and extensively observed in elliptical galaxies (Davies et al. 1993; Hes & Peletier 1993; Fisher et al. 1996; Gorgas et al. 1997; Vazdekis et al. 1997). The red wavelength range spans the Ca II IR triplet and was intended for the study of both indices and kinematics. Spatial resolutions of the CCDs were 0.78 and 0.58 arcsec per pixel on the blue and red arms, respectively. Seeing was ~ 1.5 arcsec and a 1-arcsec slit was used. Flux and velocity standard stars were also observed. Object frames were alternated with arc lamp exposures to allow for accurate wavelength

Table 1. Data for four spiral bulges observed with the Palomar 5-m telescope. Hubble Type and B magnitudes are from de Vaucouleurs et al. (1991) (hereafter RC3). Inclinations are from Guthrie (1992). Distances are from Tully (1988) assuming $H_0 = 75 \text{ km s}^{-1} \text{ Mpc}^{-1}$. Recession velocities given are from RC3 (H I data) and this work (optical data). The velocity dispersions given (σ_v) are the averages across all data points. This is the value used for calculation of broadening required to match the Lick system (see Section 2.3).

Galaxy	Hubble Type	Inclination (deg)	Distance (Mpc)	B (mag)	Recession Velocity RC3/This work (km s ⁻¹)	σ_v (km s ⁻¹)	Scale (pc arcsec ⁻¹)
NGC 2654	Sab	90	23.3	12.8	1341/1320	136	110
NGC 3623	Sa	79	7.3	9.6	807/809	152	35
NGC 4565	Sb	90	9.7	10.3	1227/1235	155	46
NGC 5689	S0/a	78	35.6	12.7	2160/2221	149	168

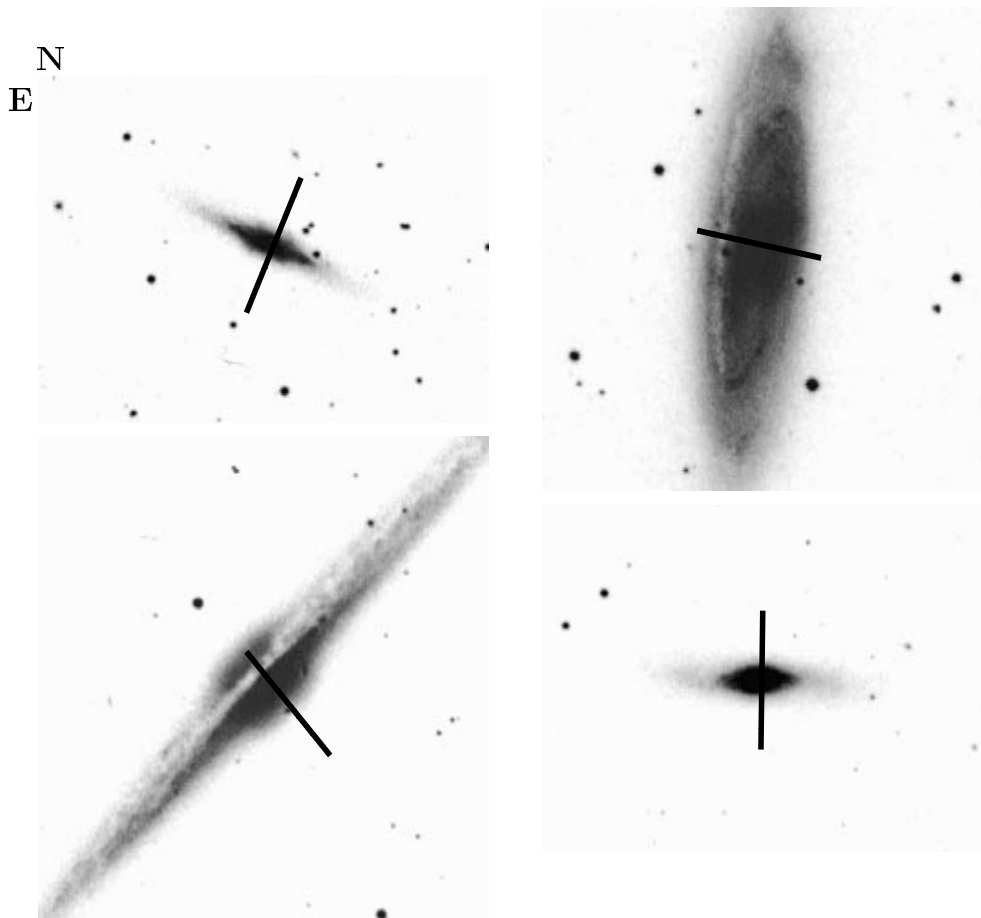


Figure 1. Digital Sky Survey images of galaxies with slit positions along minor axes. The slitlength is 2 arcmin in all images. Slit position was determined by assuming the slit passes through the telescope pointing position along the minor axis. The location of the bulge within the slit was determined by ensuring that the peak of the luminosity profile on the slit matched the position of the maximum count rate on the CCD. Upper left: NGC 2654. Note that the slit appears off-centre by approximately 5 arcsec. Upper right: NGC 3623. Sky is not reached on either side of the galaxy. However, the sky was estimated from extreme edges of slit (see Section 2.2). Lower left: NGC 4565. Sky is not reached on the side of the galaxy most affected by the disc. However, a reasonable sky estimate is achieved on the side least affected by disc. Lower right: NGC 5689. Note the slit appears off-centre by approximately 5 arcsec.

calibrations. Frames of a continuum source (tungsten lamp) were also obtained for the purpose of flat-fielding. Galaxy exposure times of 5900, 7200, 4200 and 1200 s were obtained for NGC 2654, 3623, 4565 and 5689, respectively. A maximum single-exposure time of 2400 s was adopted to facilitate cosmic ray removal.

2.2 Data reduction

Unless otherwise stated, data reduction was carried out using the FIGARO package of Starlink software. A bias level from the over-scan region was subtracted from each frame. Due to the presence of localized features in the flat-field frames, each object was divided by the normalized, average flat-field. This biases the data with the spectral response of the tungsten lamp. However, this is smooth and is removed during flux calibration. Cosmic rays were removed by interpolation between adjacent pixels. Wavelength calibration was achieved by interpolating between arc lamp exposures bracketing galaxy frames and was accurate to $\sim 0.1 \text{ \AA}$. Spectra were then flux calibrated and extinction corrected. For NGC 2654, 3623 and 5689 sky subtraction was carried out by interpolation across the galaxy. For NGC 3623 sky was not fully attained on either side of the galaxy. This results in a small

contribution of disc light to the sky estimate. The error associated with this sky was estimated from the 1σ variation in index values when sky estimates from successive galaxy exposures (NGC 2654, 3623 and 4565) were used. For NGC 4565 sky was only reached along the slit on one side of the bulge. In this case the sky was estimated from just this side of the galaxy. Variation of the sky across the slit was shown to be less than 10 per cent of sky level for frames clearly reaching sky on both sides. Finally, galaxy frames were shifted and co-added to form a single frame for each galaxy.

2.3 Measurement of kinematics and indices

Kinematics were measured in order to correct our data to the dispersion of the Lick system. Measurements of kinematics were carried out on both red and blue data using both cross-correlation and Fourier quotient techniques within the IRAF software package. Results of the two techniques were in agreement to within 5 km s^{-1} . However, the Fourier quotient technique was used because the statistical errors associated with cross-correlation were substantially larger due to the insensitivity of this method at the low-velocity dispersions typical of spiral bulges. As velocity dispersions in our sample are all less than the dispersion required

Table 2. Error table for NGC 3623. Top: index values for the central 3 arcsec and the associated Poisson noise are given. Sky errors are derived as detailed in Section 2.4. Calculations of both velocity dispersion and recession velocity errors (σ and v respectively) assume approximate velocity uncertainties of $\pm 35 \text{ km s}^{-1}$. Total errors are Poisson, sky, σ and v errors added in quadrature. Comparison to HD 139669 represents published Lick values minus values obtained from our observation of this star. These offsets are not included in the calculation of total error due to their uncertainty. Bottom: error table for outer regions (~ 8 arcsec from centre) of NGC 3623.

CENTRAL VALUES							
Index	Index Value	Poisson Noise	Sky Error	σ Error	v Error	Total Error	Comparison with HD 139669
Fe4668	8.64 Å	0.07	0.05	0.05	0.06	0.12	0.15
H β	1.29 Å	0.03	<0.01	0.03	0.02	0.05	0.60
Fe5015	4.91 Å	0.07	0.07	0.23	0.04	0.25	-0.93
Mgb	4.51 Å	0.04	0.02	0.09	0.02	0.10	-0.03
Fe5270	3.31 Å	0.04	0.01	0.10	0.01	0.11	-0.47
Fe5335	3.07 Å	0.05	<0.01	0.17	0.02	0.18	0.14
Mg ₁	0.133 mag	0.002	<0.001	0.001	<0.001	0.002	0.014
Mg ₂	0.279 mag	0.002	<0.001	0.001	0.001	0.002	0.016
OUTER VALUES							
Fe4668	6.88 Å	0.12	0.28	0.07	0.05	0.32	0.15
H β	1.22 Å	0.06	0.01	0.01	0.01	0.06	0.60
Fe5015	3.47 Å	0.12	0.47	0.21	0.11	0.54	-0.93
Mgb	4.12 Å	0.07	0.12	0.07	0.01	0.16	-0.03
Fe5270	2.79 Å	0.08	0.03	0.09	0.01	0.12	-0.47
Fe5335	2.59 Å	0.09	0.02	0.13	0.01	0.16	0.14
Mg ₁	0.107 mag	0.003	0.001	0.001	<0.001	0.003	0.014
Mg ₂	0.247 mag	0.004	0.003	0.001	0.001	0.005	0.016

for calibration to the Lick system, the additional broadening required (σ_b) can be calculated (assuming Gaussian profiles):

$$\sigma_b^2 = \sigma_L^2 - \sigma_i^2 - \sigma_v^2$$

The Lick resolution (σ_L) is approximately constant at 3.57 Å over the 4500–5500 Å range covered by our observations (Worthey & Ottaviani 1997). Instrumental broadening (σ_i) was estimated from arc lines and found to be 1.12 Å. Velocity dispersion broadening of the galaxy (σ_v) was estimated as the average over the whole galaxy in the blue (Table 1).

After broadening the spectra to the Lick resolution, the indices were evaluated by our own code, using the band wavelength range definitions supplied by G. Worthey on his home page. Worthey also kindly provides data with which our code could be tested. Differences between the Worthey-derived indices and our own for the provided spectra were ≤ 0.03 Å for the line features and ≤ 0.002 mag for the Mg₁ and Mg₂ molecular bands. These discrepancies are smaller than differences caused by re-calibration of Worthey's data to our wavelength resolution and are probably the result of the effects of differences in the handling of partial bins. They are also significantly smaller than the total errors (Section 2.4). A more important source of uncertainty in our data is the conversion to the Lick system (which was not flux calibrated). One of the observed velocity standards, HD 139669, is also one of the Lick calibration stars. Indices derived from our observations of this star and the data of Jones (1996) (data available on AAS CD-ROM Series Vol. VII) were compared to the Gorgas et al. (1993) published data. Differences between indices derived from our data and those of Jones are typically within the error range. However, there is a large discrepancy between our measurement and the published Lick data for the H β and Fe5015 indices (also reproduced in the data of Jones), which is probably caused by unpredictable wavelength shifts in the Lick IDS spectra

(Gorgas, private communication). Differences between our measured indices and the published Lick data for this star are given in Table 2. HD 139669 (HR 5826) also lies well away from the mean in fig. 10 of Gorgas et al. (1993). Therefore, this star is not suitable for estimation of correction factors to the Lick system. Lack of sufficient data to fully calibrate to the Lick system represents a limitation on the Palomar data set. However, corrections to the narrow line features discussed here (Fe4668, H β , Fe5270 and Fe5335) have been shown to be small (Gorgas et al. 1997; Vazdekis et al. 1997; Worthey & Ottaviani 1997). For Jones' (1996) observations correction to the flux-calibration-sensitive Mg₂ index was found to be small (0.01 mag increase in the measured Mg₂ index). The good agreement between our measurement of the Mg₂ index of HD 139669 and that of Jones suggests that our correction factor to the Lick system should be of similar magnitude ($\sim +0.01$ mag), although we have not applied this correction.

Initial measurements of indices showed unusual gradient inversions in the Ca II, Mg₁ and Mg₂ indices at the centres of the bulges (defined as the peak in brightness). These were found to be the result of focus variation caused by distortion of the CCD surface. This effect redistributes flux spatially between bins, introducing false continuum variations. Ca II and molecular band indices are sensitive to this type of distortion due to the large separation of their sidebands. The problem was most pronounced in the red (this CCD has subsequently been replaced at Palomar). As a result, line strength measurements were not carried out on the red arm data. Kinematic analyses were still possible, as the continuum shape is removed prior to line-broadening measurement. Stellar data from the blue arm had a smooth point source FWHM variation of < 20 per cent across the wavelength range. Even so, features are still introduced in the Mg₁ and Mg₂ indices in the centre of the galaxies where luminosity gradients are greatest. A minimum binning of ~ 1.5 arcsec has minimized this

effect and matched the seeing conditions. Central values for the purposes of modelling and comparison to ellipticals were calculated using the central 3 arcsec (see Section 3.2).

2.4 Estimation of errors

Detailed analysis of errors affecting NGC 3623 are shown in Table 2 for illustration. For all galaxies, binning of data was selected to maintain an approximately constant Poisson error outside the central regions. For NGC 2654, 4565 and 5689, sky errors were evaluated by varying the region of sky used for sky estimation. The 1σ variation in estimated index value is taken as the error. For NGC 3623, which failed to reach sky on both sides of the galaxy, sky error was estimated as the 1σ variation in indices derived utilizing sky estimates from NGC 3623 and the bracketing observations of NGC 2654 and 4565. Variation of both velocity dispersion and recession velocity about the assumed average values (Table 1) were both $\sim\pm 35 \text{ km s}^{-1}$. These variations are significantly larger than errors associated with wavelength calibration and statistical errors from the Fourier quotient technique ($\sim 9 \text{ km s}^{-1}$). Consequently, velocity dispersion errors were estimated as the variation in indices caused by increasing the galaxy velocity dispersion assumed in calculation of broadening to the Lick system by 35 km s^{-1} . Index errors due to recession velocity uncertainty were estimated as the variation in indices caused by increasing the redshift estimate by 35 km s^{-1} .

The magnitude of the sky error varied between galaxies. Consequently, unless otherwise stated, figures and tables show combined Poisson and sky errors. Velocity dispersion and recession velocity errors for other galaxies were similar in magnitude to those in NGC 3623. In the centres of the bulges Poisson noise and velocity dispersion errors dominate. While for

most cases sky error dominates in the outer regions, total errors in Fe5270 and Fe5335 continue to have significant contributions from velocity dispersion error. Gradient errors given in Table 3 were estimated as the statistical errors associated with linear fitting.

3 RESULTS

3.1 Kinematics

Results of recession velocity and velocity dispersion analysis are shown in Fig. 2. Galaxy centres are defined as the position of the luminosity peak along the slit. Reasonable agreement exists between results for red and blue data with average values for both recession velocity and velocity dispersion differing by less than 20 km s^{-1} . However, systematic differences are present in the centres of NGC 3623 and 4565. Central recession velocities derived from the red data are highly susceptible to systematic error due to focus variation (Section 2.3). Consequently, analysis of indices has been based on the blue recession velocity data only. In NGC 4565 (a known LINER: Keel 1983), the maximum in the blue velocity dispersion profile is offset by ~ 5 arcsec with respect to both the luminosity and metallicity peaks (see Figs 2 and 3). This would appear not to be an internal extinction effect as metallicity continues to rise with luminosity to the centre. Photometric observations in the near-infrared of NGC 4565 (Rice et al. 1996), rather than indicating reddening by dust in the centre, show a flattening of the colour gradient that is evident along the minor axis at distances greater than 5 arcsec (Rice et al. 1996; fig. 2a). The change in colour gradient is coincident with the peak in blue velocity dispersion data in Fig. 2 and the edge of the broad metallicity peak in Fig. 3. The central region of radius 5 arcsec is also the emission region of NGC 4565. Strong [O III]

Table 3. Top: central 3 arcsec index values (except H β for NGC 4565 where the average of outer values is used to avoid emission: see Section 3.2). Errors (given in brackets) are Poisson noise and sky errors combined. Middle: index gradients calculated from all available data points. For NGC 4565, errors are statistical errors (associated with linear fitting technique) combined with uncertainty in position of the galaxy centre. Positional uncertainties are small in other galaxies; consequently, for these, quoted errors are purely statistical errors. Bottom: central velocity dispersions. Quoted errors are statistical errors from the Fourier quotient technique.

Central index values				
	NGC 2654	NGC 3623	NGC 4565	NGC 5689
Fe4668 (\AA)	7.33(0.25)	8.64(0.08)	8.94(0.17)	8.72(0.26)
H β (\AA)	1.47(0.09)	1.29(0.03)	1.49(0.08)	1.98(0.11)
Fe5015 (\AA)	4.69(0.27)	4.91(0.10)	2.49(0.16)	5.74(0.24)
Mgb (\AA)	4.13(0.11)	4.51(0.04)	4.67(0.08)	4.03(0.13)
Fe5270 (\AA)	3.00(0.12)	3.31(0.04)	3.32(0.09)	3.00(0.14)
Fe5335 (\AA)	2.67(0.14)	3.07(0.05)	3.14(0.10)	2.62(0.16)
Mg ₁ (mag)	0.105(0.005)	0.133(0.002)	0.139(0.004)	0.095(0.006)
Mg ₂ (mag)	0.244(0.007)	0.279(0.002)	0.293(0.005)	0.237(0.008)
Index gradients [δ Index/ $\delta \log(\text{radius})$]				
(Fe)	-0.60(0.44)	-0.44(0.05)	-0.58(0.10)	-0.55(0.19)
Fe4668	-0.61(0.98)	-1.89(0.14)	-2.20(0.33)	-3.28(0.60)
Mg ₂	-0.022(0.016)	-0.032(0.003)	-0.061(0.008)	-0.027(0.012)
H β	-0.35(0.21)	-0.06(0.04)	0.52(0.11)	0.25(0.20)
Central velocity dispersions				
σ_0 (km s^{-1})	145(7)	145 ¹ (7)	162 ² (7)	147(8)

¹ Peak value 175 km s^{-1} at 5 arcsec off-centre.

² Peak value 190 km s^{-1} at 5 arcsec off-centre.

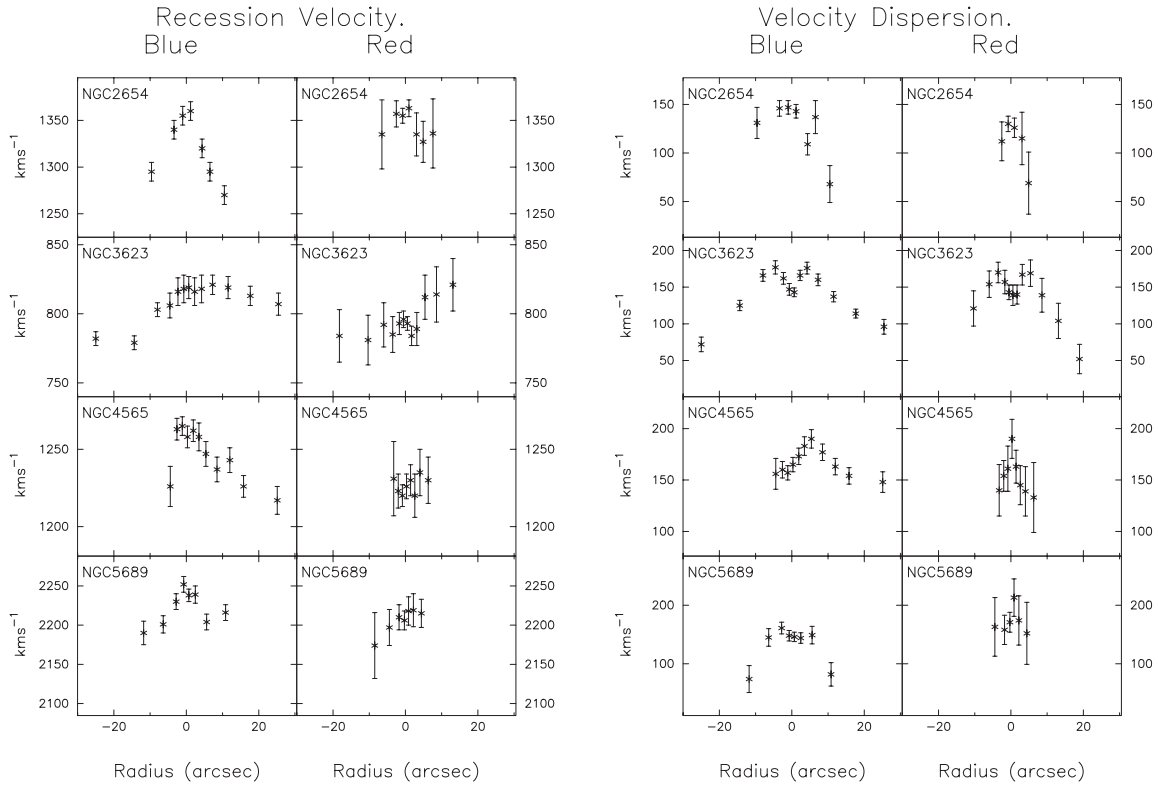


Figure 2. Spatially resolved kinematics along the minor axes of four spiral bulges. Recession velocities and velocity dispersions from both the blue and red Palomar data are shown. Both sets of data were derived by the Fourier quotient technique. Error bars represent statistical errors of this technique and do not include systematic errors.

5007- and 4959-Å emission lines are present in this region affecting the Fe5015 index, while the $H\beta$ index exhibits features due to emission-line filling (Fig. 3). Thus, the data suggest that the core of NGC 4565 contains a blue, metal-rich, kinematically cold subpopulation perhaps associated with ongoing star formation. The presence of such a population would also cause a displacement between red and blue luminosity peaks as observed.

A dip in velocity dispersion is seen in the centre of NGC 3623 and is reproduced in both red and blue data sets. Such velocity dispersion profiles have been observed along the major axis of spiral galaxies (e.g. Bertola et al. 1996; Bottema & Gerriston 1997). Kinematic models that reproduce such dips in velocity dispersion include the presence of a kinematically distinct component within the bulge such as an isothermal nuclear core (Bottema & Gerritsen 1997), a disc (Bertola et al. 1996) or a bar (Friedli 1996). Chemodynamical modelling of the effect of the presence of a bar on disk galaxies (Friedli 1998) has shown that metallicity gradients are reduced in the plane of the bar around and outside the region of the corotation radius, while steeper gradients can occur at radii well within corotation. A flattening of the metallicity gradients is also induced along the minor axis. The gradients in metallicity-sensitive indices along the minor axis of NGC 3623 (Fig. 3), which flatten rapidly away from the centre, are consistent with such models. Friedli, Benz & Kennicutt’s (1994) models also predict inflow of gas within the corotation radius resulting in a central burst of metal-rich star formation. The sharp metallicity peak, evident in both Fe and Mg indices in Fig. 3, may be the result of this process. Photometric observations by Burkhead & Hutter (1981) and recent Hubble archive images of NGC 3623 show boxy central isophotes, which may also be

indicative of the presence of a bar. Alternatively, the kinematic feature may be the result of an embedded stellar disc. If this is the case, either the disc has a scaleheight of ~ 150 pc (major axis disc) or the disc rotates along the minor axis with a radius of ~ 150 pc. However, there is no evidence of the kinematic signature of a minor axis disc on this scale in the recession velocity measurements (Fig. 2). On balance it would seem likely that the centre of this spiral bulge harbours a small-scale bar. (Note also that RC3 gives the classification of NGC 3623 as SXT1. This indicates a ‘mixed’ bar/no bar type.)

As all the indices described here are from the blue data, and the red data suffer degradation by focus variation, we have used the blue velocity dispersion and recession velocity values in our analysis of the indices. Average values across the galaxies were used for both recession velocity and velocity dispersion in recognition of the systematic uncertainties. The resultant recession velocities are in good agreement with values given in RC3 (Table 1).

3.2 Lick indices

In this section we present the results of index evaluations and plot the data on several diagnostic plots for comparison to models of SSPs and observations of other galactic morphologies. Index measurements across the four bulges are shown in Table 3 and Fig. 3. Negative radial gradients can be seen in all the metallicity-sensitive indices with the possible exception of Fe5015, which is strongly affected by the [O III] 5007-Å emission line. Mg b is affected by emission of the [N I] 5199-Å doublet in one of the sidebands (Goudfrooij & Emsellem 1996). However, the

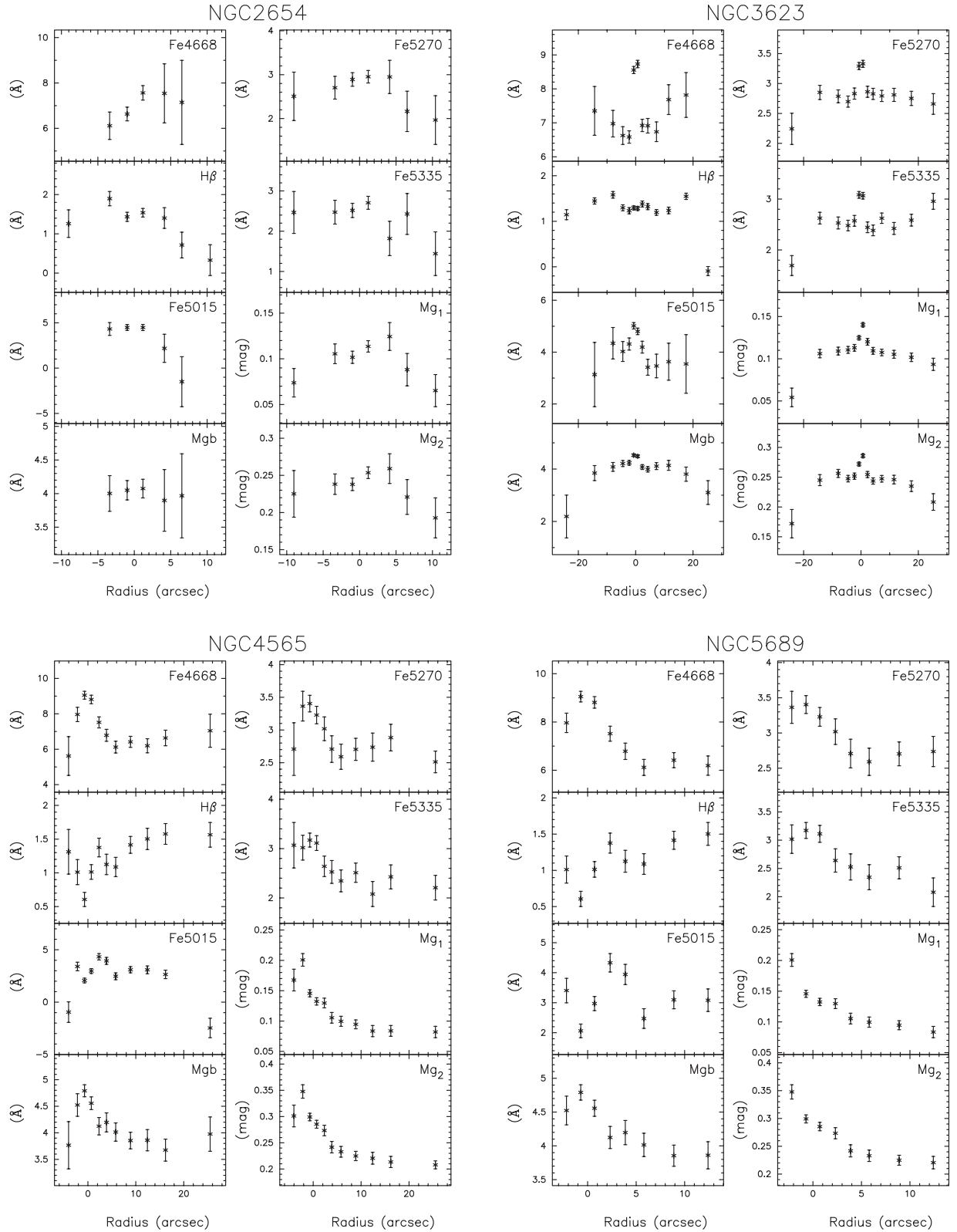


Figure 3. Indices across the minor axes of four spiral bulges. Radial gradients can be seen in most metallicity-sensitive features. The central dips in H β in NGC 4565 are the result of emission. Fe5015 is also emission affected. The errors bars shown include Poisson noise and sky error only. Bin sizes were selected so as to maintain approximately constant Poisson error values beyond the central pixels. The increasing influence of the sky error at large radii can be seen. Note the sharp central peak in metallicity-sensitive indices in NGC 3623. This peak coincides with a dip in central velocity dispersion.

enhancement of this index caused by emission appears to be small in these data for all galaxies, with the possible exception of the LINER NGC 4565. The age-sensitive $H\beta$ index can also suffer from emission-line filling, particularly near the centres of bulges. This is most clearly seen in NGC 4565 (Fig. 3). Dips in $H\beta$ at the centre of this galaxy are associated with two separate emission regions and are reflected by features in the Fe5015 index. The dip in $H\beta$ in the central region of NGC 3623 may also indicate weak emission. However, this galaxy exhibits sharp central peaks in metallicity-sensitive features that coincide with a dip in the velocity dispersion (see Section 3.1). The combined effects of the influence of the metallicity peak and emission on the $H\beta$ index in the centre of this galaxy makes interpretation difficult. The symmetry of indices about galaxy centres indicates that only in NGC 4565 is disc obscuration significant.

Fig. 4 shows central values of Mg_2 versus $\langle Fe \rangle$ for our four spiral bulges. Also plotted are central index values of elliptical (E) and Sph galaxies (Gorgas et al. 1997), S0 galaxies (Fisher et al. 1996) and the bulge of M104 (Hes & Peletier 1993). This diagram illustrates trends in the relative abundance and abundance ratio of different morphological types. Dotted lines indicate the extent of the space occupied by Worthey's solar abundance ratio SSPs and the solar metallicity locus. The high central strengths of the $\langle Fe \rangle$ index found in E and S0 galaxies are also apparent in spiral bulges, with bulge indices comparable to those of SSPs with solar metallicity or above. Fig. 4 also demonstrates that the cores of Es exhibit Mg_2 values in excess of those possible for SSPs with Salpeter IMF and solar abundance ratios. This is the well-known Mg excess in elliptical galaxies discussed in Section 1. S0 galaxies lie *intermediate* between Es and the SSPs. The position of the four spiral bulges is consistent with solar abundance ratios. This is in

agreement with the result of Sil'chenko (1993) and Worthey's (1998) interpretation of the Jablonka et al. (1996) data for bulges. Outer regions of the bulges are also consistent with solar abundance ratio SSPs (Sansom, Proctor & Reid 1998). Analysis of the flux-calibrated data of Jones (Worthey & Ottaviani 1997) indicated additive corrections of +0.01 mag and -0.06 \AA for calibration of Mg_2 and $\langle Fe \rangle$ features respectively to the Lick system. While reasonable values for this correction for the Palomar data may move some of the spiral bulge data points just outside the region of solar ratio SSPs, the conclusion that Mg is significantly underabundant in spiral bulges, when compared to ellipticals, remains unchanged. The bulge of M104 (Hes & Peletier 1993) does not appear to follow the trend suggested by our sample (Fig. 4), but instead falls amongst the elliptical galaxies. Therefore, these data support the suggestion by Hes & Peletier, that the bulge of M104 (classified as S0/a in RC3) more closely resembles an elliptical galaxy than a normal spiral bulge.

In Fig. 5 we plot $\langle Fe \rangle$ against $H\beta$. This diagram provides evidence relating to the relative ages of stellar populations. The correction factors to transform flux-calibrated $H\beta$ data to the Lick system have been shown to be small (Worthey & Ottaviani 1997). Index values from our data are from the central 3 arcsec, except for NGC 4565 where the average outer $H\beta$ value was used (omitting central values where this index is emission affected). We therefore assume no significant gradient in $H\beta$ for NGC 4565. This is consistent with studies of elliptical galaxies (Carollo et al. 1993; Davies et al. 1993; Fisher, Franx & Illingworth 1995; Fisher et al. 1996; Gorgas et al. 1997; Vazdekis et al. 1997) that show no detectable age gradients. The possible presence of emission in the bulges creates uncertainty in the reliability of our $H\beta$ determination, making interpretation of this index difficult. However, it

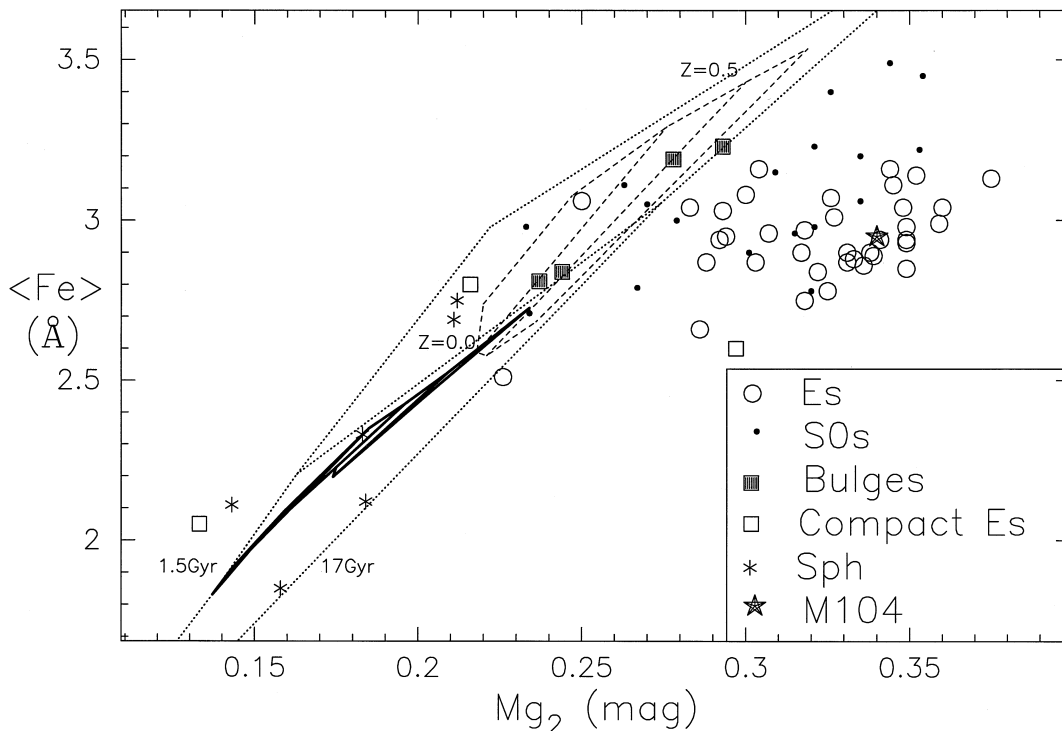


Figure 4. Mg_2 versus $\langle Fe \rangle$ for elliptical and Sph galaxies (Gorgas et al. 1997) and S0 galaxies (Fisher et al. 1996). Results for the four spiral bulges presented here and the bulge of the Sa galaxy M104 (Hes & Peletier 1993) are also shown. The dotted lines indicate the extremes of Worthey's (1994) SSPs and also the solar metallicity locus ($Z = 0.0$). The solid lines indicate the range of index values achieved by primordial collapse models with a range of star formation efficiencies from 0.2 to 4.0 Gyr^{-1} (described in Section 4). Dashed lines indicate index values achieved by a range of extended inflow models with star formation efficiencies of 4.0 Gyr^{-1} over 4 to 6 Gyr. Ages of 5, 8, 12 and 17 Gyr are shown. All models plotted assume solar abundance ratios.

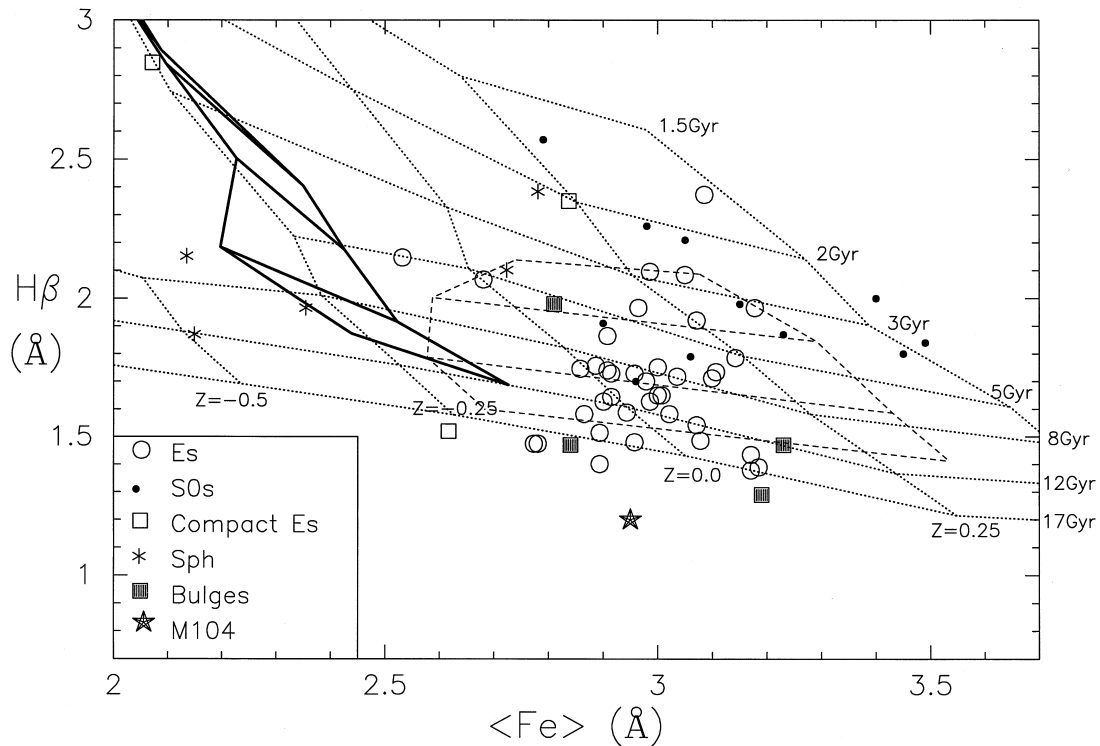


Figure 5. $\langle \text{Fe} \rangle$ versus $H\beta$ for E, S0 and Sph galaxies as well as M104 and the four spiral bulges presented here. Data sources are as in Fig. 4. Dotted lines indicate Worthey's SSP, with values of $Z = [\text{Fe}/\text{H}]$; -0.5 , -0.25 , 0.0 , $+0.25$, $+0.5$ and ages 1.5, 2, 3, 5, 8, 12 and 17 Gyr. It must be noted that due to the effects of emission on the central $H\beta$ index for NGC 4565 and M104, the plotted $H\beta$ values are averaged outer values. Solid and dashed lines are as described in Fig. 4 (see Section 4).

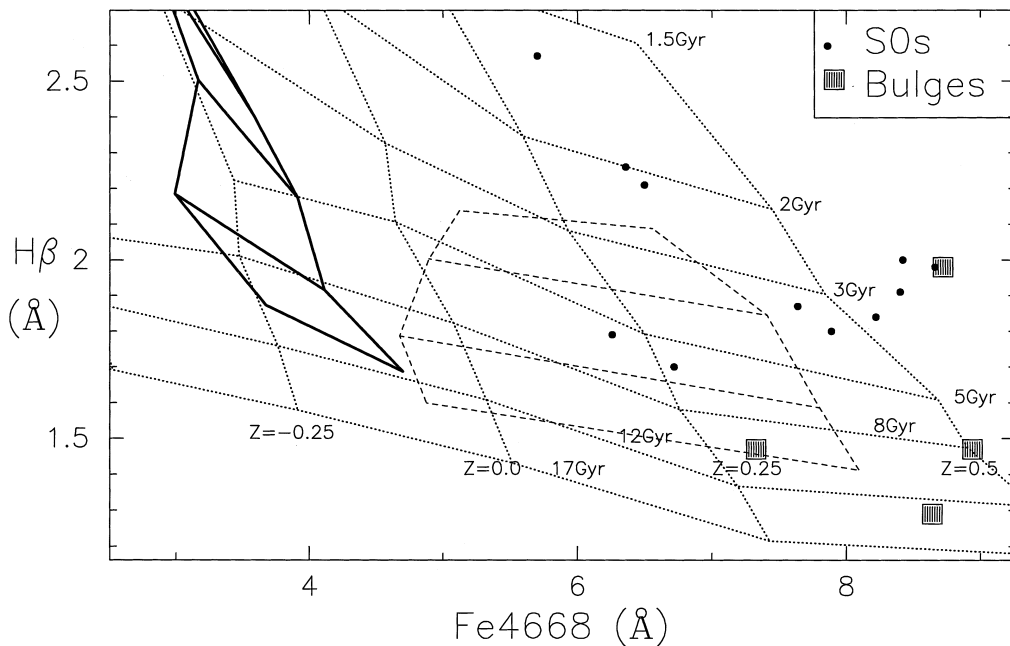


Figure 6. $H\beta$ versus Fe4668 for S0 galaxies (Fisher et al. 1996) and the four spiral bulges presented here. [N.B. Gorgas et al. (1997) did not include Fe4668.] Dotted lines indicate Worthey's SSP values for metallicities: -0.25 , 0.0 , $+0.25$, $+0.5$ and ages of 1.5 to 17 Gyr. Solid and dashed lines are as in Fig. 4 (see Section 4).

should be noted that NGC 5689 (with $H\beta \sim 2.0 \text{ \AA}$) shows no sign of central emission which, in any case, would only *increase* the estimate of $H\beta$ for the underlying population. Thus, the strong $H\beta$ in this galaxy is compelling evidence of an intermediate age (≤ 5 Gyr) population.

Fig. 6 locates the spiral bulges in the Fe4668 versus $H\beta$ plane. The Fe4668 index is extremely metallicity-sensitive (Worthey 1994). The correction factor to transform Fe4668 to the Lick system has been shown to be small (Worthey & Ottaviani 1997). Comparison of Figs 5 and 6 illustrates that higher metallicities are

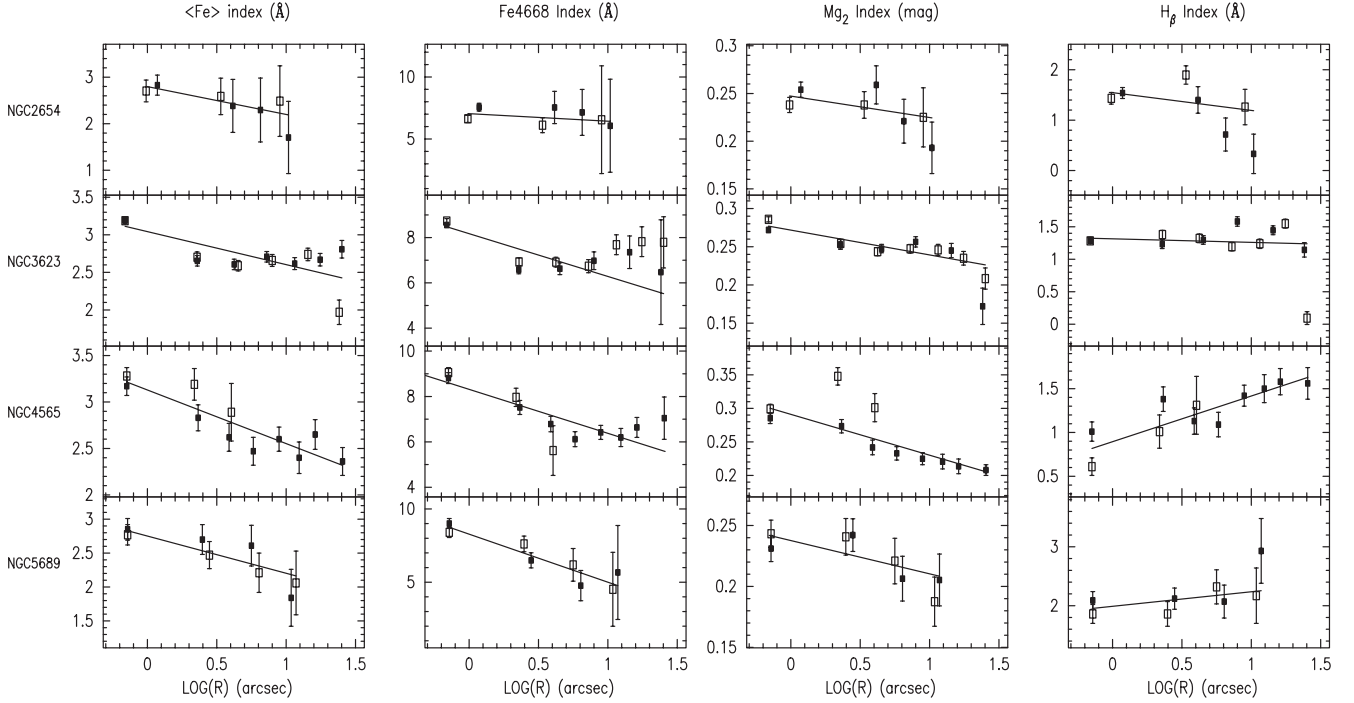


Figure 7. Index versus log radius (radius in arcsec) for $\langle\text{Fe}\rangle$, Fe4668, Mg_2 and $\text{H}\beta$ indices of the four galaxies of the Palomar data set. Open squares are the disc-contaminated side of the galaxies. All data points within the regions spanned by the regression lines are included in the fit. Note the flattening in metallicity-sensitive indices in NGC 3623 which may be associated with the presence of a bar.

suggested by Fe4668 than by $\langle\text{Fe}\rangle$. As the Fe4668 index is highly carbon sensitive (Tripicco & Bell 1995), this may indicate either an abundance ratio difference or a problem with the calibration of Fe4668. The main source of carbon enrichment of the ISM is still controversial. Gustafsson et al. (1999) report falling $[\text{C}/\text{Fe}]$ with increasing $[\text{Fe}/\text{H}]$ in the solar neighbourhood. They suggest that high-mass stars are the major contributors of C to the ISM. However, both intermediate- and low-mass stars are also known to produce C. Consequently, the interpretation of a C overabundance is difficult. It must also be noted that at high metallicities the value of this index changes rapidly with metallicity. It is possible that the seeming Fe4668 excess is in fact the result of the lack of calibrated SSP data at metallicities greater than $[\text{Fe}/\text{H}] = 0.5$. Caution is advised in interpreting this index at high metallicities.

3.3 Gradients in indices and correlations

Gradients were estimated by least-squares fitting for the $\langle\text{Fe}\rangle$, Fe4668, Mg_2 and $\text{H}\beta$ indices plotted versus log radius from the galaxy centre (Fig. 7). Data from both sides of the galaxies were included in these fits. The gradients obtained are given in Table 3. Central galaxy regions are marginally affected by seeing. However, central index values were included in the gradient estimates due to the limited number of data points. As gradients are unaffected by a constant offset to convert to the Lick system, a direct comparison with elliptical galaxies can be made. Gradients, central Mg_2 values and central velocity dispersions (σ_0 : Table 3) of the bulges are consistent with the correlations reported by Carollo et al. (1993) in elliptical galaxies. The bulges show Mg_2 gradients of similar magnitude to those in elliptical galaxies possessing the same central velocity dispersions and central Mg_2

values. The gradients are also similar in magnitude to those reported in Sansom, Peace & Dodd (1994) for two bulges (NGC 3190 and NGC 1023). The central velocity dispersions and the central index values of our Palomar sample, indicating solar abundance ratios, are also consistent with the pattern suggested by Worthey (1998) that *all* spheroids with velocity dispersions of less than 225 km s^{-1} possess solar $[\text{Mg}/\text{Fe}]$.

4 MODELLING CENTRAL LINE STRENGTHS

In order to investigate possible SFHs, we use our galactic chemical evolution (GCE) code detailed in Sansom & Proctor (1998). Briefly, the model calculates star formation rate (SFR) and the metallicity of the gas at each time-step throughout the history of the region being modelled. As all stars formed in each time-step are of the same age and metallicity, they constitute an SSP. Composite indices are then calculated as the luminosity-weighted sum of indices from interpolations between tabulated SSP values of Worthey (1994) which cover populations of age 1.5 to 17 Gyr. The code currently models a single zone allowing for gas inflow. The rate of gas inflow can be varied and can be either primordial or enriched to the same level as the gas already in the region (simulating inflow from a neighbouring region with similar SFH). SFR is assumed to be proportional to some power (α) of the gas mass density (ρ); $\text{SFR} = C\rho^\alpha$, where C is the star formation efficiency (Gyr^{-1}) if $\alpha = 1$. Kennicutt (1989) shows that the value of α in galactic discs lies between 1 and 2. In all models presented here we assume $\alpha = 1$ and inflow is enriched. The differences in indices caused by assuming $\alpha = 2$ were shown to be small and make no significant difference to the conclusions for the models presented here. The code permits the modification of the star

formation efficiency and inflow rates at two points in the history of the galaxy. In this way various formation scenarios can be modelled. The star formation efficiency modelled ranges between values for typical Sb galaxies ($C = 0.2$) up to those for starburst galaxy types ($C = 4$). In order to follow the enrichment of the gas by feedback mechanisms, such as SNII, SNIa and mass loss from intermediate-mass stars, the total metal content of the gas is traced in a self-consistent manner. Data for SNII (high-mass stars) were taken from Woosley & Weaver (1995) and Maeder (1992). SNIa data are from Nomoto, Thielmann & Yokoi (1984). For intermediate-mass stars Renzini & Voli (1981) data were used. The code also uses the SSPs of Weiss, Peletier & Matteucci (1995) to estimate the effects of non-solar abundance ratios on $\langle \text{Fe} \rangle$ and Mg_2 predictions. Currently, our GCE code outputs estimates of 21 Lick indices for the population being modelled.

4.1 Primordial collapse

Primordial collapse represents the isolated collapse of a primordial gas cloud. The cloud commences star formation when the local density rises above some critical level. This mechanism has been proposed for the formation of elliptical galaxies. Dynamical models of elliptical galaxy formation by primordial collapse (Carlberg 1984) show that the period of gas inflow is < 1 Gyr. The chemodynamical models of Theis et al. (1992) also show the main burst of star formation to be complete in ≤ 1 Gyr. Thus, these models predict an SFH comprising a single burst of star formation with a large majority of stars formed within the first 1 Gyr. This naturally leads to the prediction of $[\text{Mg}/\text{Fe}] >$ solar, observed in the centres of elliptical galaxies, as there is insufficient time for SNIa to contribute large quantities of Fe to the ISM before the bulk of star formation is complete. These models also successfully predict many photometric properties such as the de Vaucouleurs $r^{1/4}$ profile and the presence of colour (metallicity) gradients. However, several authors (Worthey et al. 1996; Greggio 1997; Vazdekis et al. 1997; Sansom & Proctor 1998) have shown that primordial collapse models fail to reproduce the strong central, metallicity-sensitive, line strengths found in elliptical galaxies, under the assumption of a constant, Salpeter IMF. This is the result of the high number of low-metallicity stars produced in this scenario. We find this to be true also for the centres of spiral bulges which exhibit metallicities similar to the centres of elliptical galaxies (Fig. 4). To demonstrate this point we have calculated indices for a range of primordial collapse models. Parameters within the models were set to maximize predicted central metallicities while keeping models realistic. Thus, as infall of primordial gas into the modelled region would dilute the metals content of the star-forming ISM, we assumed enriched inflow. The gas flow rate per Gyr was set to 10 times the initial gas content of the region. As the inflow is enriched, this large value ensures that the number of low-metallicity stars produced is kept small. Significantly higher values of inflow rate had negligible effects on the achieved line strengths. To be consistent with dynamical models of primordial collapse the period of inflow was stopped after 0.4 Gyr while the star formation was allowed to continue to the present day, albeit at an ever decreasing rate as gas is consumed. This generates an ~ 1 Gyr burst of SF, which is also consistent with the chemodynamical models of Theis et al. (1992). Continuation of star formation to the present day also maximizes the predicted strengths of metallicity-dependent lines. To demonstrate the range of metallicities such models can achieve, star formation efficiency

(C) during the inflow period was varied between 0.2 and 4.0 Gyr^{-1} . This range of star formation efficiencies spans the values given by Fritz-v. Alvensleben & Gerhard (1996) for Sb, Sa and E galaxies up to values for ultraluminous starburst galaxies. After the initial 0.4 Gyr of inflow, star formation was allowed to continue in all models with an efficiency $C = 0.2$. The ages of the models varied between 1.5 and 17 Gyr. The results of our GCE models of primordial collapse for $\langle \text{Fe} \rangle$, Mg_2 , $\text{H}\beta$ and Fe4668 are shown as solid lines in Figs 4 to 6. Comparison of indices for E, S0 and spiral bulges (Fig. 4) to the range of values achieved by primordial collapse models shows the inability of these models to reproduce the observed central line strengths for both $\langle \text{Fe} \rangle$ and Mg_2 features. This result is confirmed in Figs 5 and 6. Introduction to models of a biased IMF at early epochs can resolve the underabundance problem but cannot simultaneously explain the high $\text{H}\beta$ values observed in some elliptical galaxies and at least one of our spiral bulges (Fig. 5). We might also expect to see an Mg_2 excess with respect to solar in the biased IMF scenario. There is no evidence for this excess in our bulge data.

4.2 Merger models

While direct evidence for primordial collapse is not observed, examples of ongoing galaxy mergers are. Indeed, Schweizer & Seitzer (1992) suggest that, based on the number of galaxies exhibiting ongoing mergers or the fine structure indicative of a recent event, ~ 50 per cent of field ellipticals have undergone a merger event in the last 7 Gyr. This would seem to be supported by the fact that ~ 50 per cent of the elliptical and S0 sample shown in Fig. 5 show $\text{H}\beta$ values that lie *above* the 8-Gyr SSP line. In merger models, galaxy formation proceeds by coalescence of fragments that have undergone star formation prior to merger. Such models can achieve high central line strengths as the period of star formation prior to merger pre-enriches the ISM from which the bulk of the population is formed (Sansom & Proctor 1998). It should be noted that both primordial collapse and merger models of galaxy formation predict short bursts of star formation due to the extremely rapid inflow of gas in both scenarios (Theis et al. 1992; Barnes & Hernquist 1996). Therefore, the excess Mg observed in elliptical galaxies is predicted by both of these models, without the need for the assumption of a biased IMF. The modelling of spiral bulges, using merger models, is constrained by their lack of Mg_2 excess. As the time-scale of gas inflow during an interaction is extremely rapid, large merger-induced starbursts will result in an Mg_2 excess. As this is not seen in our spiral bulges, if bulge formation is dominated by accretions/mergers, the star formation bursts must have been small and numerous. This is consistent with the presence of the disc, which is highly unstable to mergers of more than a few per cent of the total galaxy mass (Tóth & Ostriker 1992). While we can construct single-burst merger models that reproduce the $\langle \text{Fe} \rangle$, $\text{H}\beta$ and Mg_2 indices observed in the bulges, detailed modelling of merger scenarios has not been carried out as the large parameter space implied by multiple short bursts makes these models highly degenerate. In the limiting case, where interactions are so frequent that the induced star formation is effectively continuous, we expect merger models converge to extended inflow models.

4.3 Models with extended inflow

Extended-inflow models represent long-term inflow of gas into the region being modelled (e.g. Samland, Hensler & Theis 1997). The

long duration of the inflow is consistent with formation of the bulge both by infall of gas from the disc (perhaps by the action of bars) as well as by the accretion of gas from the halo or captured satellite galaxies over an extended period. The models assume constant star formation efficiency (C) with relatively modest gas inflow over a period of 2 to 17 Gyr and model spectral indices at a variety of points in the history of the population. With reasonable choices for C ($0.4\text{--}4.0\text{Gyr}^{-1}$) and inflow rate ($10^5\text{--}10^6 M_{\odot}\text{Gyr}^{-1}$) the observed $\langle\text{Fe}\rangle$, Mg_2 and $\text{H}\beta$ in bulges can simultaneously be reproduced to within the errors. An inflow rate of $10^6 M_{\odot}\text{Gyr}^{-1}$ corresponds to an increase in mass in the volume modelled equal to the initial mass every Gyr. The range of star formation efficiencies excludes low values ($0 < C < 0.4$) as, even with continuous star formation for 17 Gyr, there is insufficient star formation to produce the metals required to achieve the high central line strengths of NGC 3623 and 4565. Formation episodes of $\lesssim 2$ Gyr result in an Mg_2 enhancement not reflected in the data (using the SSP models of Weiss et al. 1995). Figs 4 to 6 show the range of indices achieved by a selection of extended-inflow models that reproduce the indices of the spiral bulges in both the Mg_2 versus $\langle\text{Fe}\rangle$ and $\langle\text{Fe}\rangle$ versus $\text{H}\beta$ planes to within the errors. However, it should be noted that the models are highly degenerate with respect to inflow rate and duration, star formation efficiency, and time of star formation onset (galaxy age). Consequently, the models are only shown to illustrate their ability to achieve the indices. The range of star formation efficiencies and inflow durations that can reproduce the $\langle\text{Fe}\rangle$, Mg_2 and $\text{H}\beta$ indices in our four bulges are consistent with the findings of Samland et al. (1997) using a chemodynamical model of disc galaxy formation. Blum et al. (1996) showed that red giants in the Galactic Bulge possess approximately solar metallicities and suggest that multiple epochs of star formation have occurred in the centre of the bulge in the last 7–100 Myr. Consequently, extended-inflow models of spiral bulge formation are, so far, entirely consistent with both observations of Lick indices, the stars in our own bulge and chemodynamical modelling.

5 CONCLUSIONS

Our study of the bulges of four spiral galaxies using the Lick system of spectral indices has shown that central line strengths are high. $\langle\text{Fe}\rangle$ indices are similar to those found in the centres of elliptical galaxies. However, a difference in Mg_2 index at a given $\langle\text{Fe}\rangle$ exists between elliptical galaxies and our sample of spiral bulges. Spiral bulges lie within the region of the Mg_2 versus $\langle\text{Fe}\rangle$ plane occupied by the solar abundance ratio SSPs of Worthey (1994), while ellipticals exhibit enhanced Mg_2 (the known $[\text{Mg}/\text{Fe}]$ excess). This difference between the two object types reflects differences in their star formation histories. Our data are consistent with both correlations of Mg_2 with central velocity dispersion and Mg_2 gradient with central velocity dispersion observed in elliptical galaxies.

Using our GCE code, we have shown that the central line strengths in spiral bulges cannot be achieved with primordial collapse models of spheroid formation with or without the assumption of constant Salpeter IMF. Indeed, the inferred solar $[\text{Mg}/\text{Fe}]$ argues against a biased IMF in spiral bulges. Models of bulge formation with gas inflow and star formation extended over 2–17 Gyr can achieve the observed central line strengths in all of our sample. These models are consistent with the chemodynamical modelling of Samland et al. (1997) as well as

observations of individual stars in the bulge of our own Galaxy (Minniti et al. 1992; Blum et al. 1996). It has been shown that at least one bulge (NGC 5689) must contain a population of relatively young stars ($\lesssim 5$ Gyr) again consistent with extended-inflow models of bulge formation.

NGC 3623 shows the presence of kinematic substructure. A dip in velocity dispersion is observed in the centre of this galaxy coincident with a sharp peak in metallicity-sensitive indices. This structure suggests the presence of a bar, or perhaps disc, at the centre of this galaxy. Analysis of a much larger sample of galaxies, including a repeat observation of NGC 3623, is being carried out with observations from the William Herschel Telescope, to test the findings of this paper. These data will be presented in a future paper and will include other age-sensitive indices, such as the newly calibrated $\text{H}\delta$ and $\text{H}\gamma$ indices, which are less affected by emission than the $\text{H}\beta$ index. Increased accuracy of age determination, coupled with the larger number of metallicity-sensitive indices, will permit tighter constraint of our models of bulge formation and their star formation histories.

ACKNOWLEDGMENTS

We thank our referee D. Friedli for his constructive comments. The authors acknowledge the data analysis facilities provide by the Starlink Project which is run by CCLRC on behalf of PPARC. In addition, the IRAF software package was used. IRAF is distributed by the National Optical Astronomy Observatories, which is operated by AURA, Inc., under cooperative agreement with the National Science Foundation. This work is based on observations obtained at Palomar observatory, which is owned and operated by the California Institute of Technology.

REFERENCES

- Balcells M., Peletier R. F., 1994, *AJ*, 107, 135
- Barnes J. E., Hernquist L., 1996, *ApJ*, 471, 115
- Bender R., Burstein D., Faber S. M., 1993, *ApJ*, 411, 153
- Bertola F., Cinzano P., Corsini E. M., Pizzella A., Persic M., Salucci P., 1996, *ApJ*, 458, L67
- Blum R. D., Sellgren K., Depoy D. L., 1996, *AJ*, 112, 1988
- Bottema R., Gerritsen J. P. E., 1997, *MNRAS*, 290, 585
- Burkhead M. S., Hutter D. J., 1981, *AJ*, 86, 523
- Carlberg R. G., 1984, *ApJ*, 286, 403
- Carollo C. M., Danziger I. J., Buson L., 1993, *MNRAS*, 265, 553
- Davies R. L., Sadler E. M., Peletier R. F., 1993, *MNRAS*, 262, 650
- de Vaucouleurs G., de Vaucouleurs G., Corwin H. G., Buta R. J., Fouque P., Paturel G., 1991, *Third Reference Catalogue of Bright Galaxies*, Springer-Verlag, New York (RC3)
- Faber S. M., Friel E. D., Burstein D., Gaskell C. M., 1985, *ApJS*, 57, 711
- Fisher D., Franx M., Illingworth G., 1995, *ApJ*, 448, 119
- Fisher D., Franx M., Illingworth G., 1996, *ApJ*, 459, 110
- Fritze-v. Alvensleben U., Gerhard O. E., 1994, *A&A*, 285, 751
- Friedli D., 1996, *A&A*, 312, 761
- Friedli D., 1998, in Friedli D., Edmunds M., Robert C., Drissen L., eds, *ASP Conf. Ser. 147, Abundance Profiles: Diagnostics Tools for Galaxy History*. Astron. Soc. Pac., San Francisco, p. 287
- Friedli D., Benz W., Kennicutt R., 1994, *ApJ*, 430, L105
- Frogel J. A., 1998, *Galaxy Evolution: Connecting the Distant Universe with the Local Fossil Record*. Observatoire de Paris-Meudon, in press (astro-ph/9812034)
- Gibson B. K., Matteucci F., 1997, *MNRAS*, 291, L8
- Gorgas J., Faber S. M., Burstein D., González J. J., Courteau S., Prosser C., 1993, *ApJS*, 86, 153

- Gorgas J., Pedraz S., Guzmán R., Cardiel N., González J. J., 1997, *ApJ*, 481, L19
- Goudfrooij P., Emsellem E., 1996, *A&A*, 306, L45
- Greggio L., 1997, *MNRAS*, 285, 151
- Gustafsson B., Karlsson T., Olsson E., Edvardsson B., Ryde N., 1999, *A&A*, 342, 426
- Guthrie B. N. G., 1992, *A&AS*, 93, 255
- Hes R., Peletier R. F., 1993, *A&A*, 268, 539
- Jablonka P., Martin P., Arimoto N., 1996, *AJ*, 112, 1415
- Jones L., 1996, PhD thesis, University of North Carolina
- Keel W. C., 1983, *ApJ*, 466, 486
- Kennicutt R. C., 1989, *ApJ*, 344, 685
- Maeder A., 1992, *A&A*, 264, 105
- Minniti D., Olszewski E., Liebert J., White S. D. M., Hill J. M., Irwin M. J., 1995, *MNRAS*, 277, 1293
- Nomoto K., Thielmann F. K., Yokoi K., 1984, *ApJ*, 286, 644
- Oke J. B., Gunn J. E., 1982, *PASP*, 94, 586
- Renzini A., Voli M., 1981, *A&A*, 94, 175
- Rice W., Merrill K. M., Gatley I., Gillett F. C., 1996, *AJ*, 112, 114
- Samland M., Hensler G., 1997, *ApJ*, Theis Ch., 476, 544
- Sansom A. E., Proctor R. N., 1998, *MNRAS*, 297, 953
- Sansom A. E., Peace G., Dodd M., 1994, *MNRAS*, 271, 39
- Sansom A. E., Proctor R. N., Reid I. N., 1998, in Friedli D., Edmunds M., Robert C., Drissen L., eds, ASP Conf. Ser. 147, Abundance Profiles: Diagnostics Tools for Galaxy History. Astron. Soc. Pac., San Francisco, p. 26
- Schweizer F., Seitzer P., 1992, *AJ*, 104, 1039
- Sil'chenko O. K., 1993, *Pis'ma Astrom. Zh*, 19, 701
- Theis C., Burkert A., Hensler G., 1992, *A&A*, 265, 465
- Tóth G., Ostriker J. P., 1992, *A&A*, 265, 465
- Tripicco M. J., Bell R. A., 1995, *AJ*, 110, 3035
- Tully R. B., 1988, *Nearby Galaxies Catalogue*. Cambridge University Press, Cambridge
- Vazdekis A., Peletier R. F., Beckman J. E., Casuso E., 1997, *ApJS*, 111, 203
- Weiss A., Peletier R. F., Matteucci F., 1995, *A&A*, 296, 73
- Woolsey S. E., Weaver T. A., 1995, *ApJS*, 101, 181
- Worthey G., 1994, *ApJS*, 95, 107
- Worthey G., 1998, *PASP*, 110, 888
- Worthey G., Ottaviani D. L., 1997, *ApJS*, 111, 377
- Worthey G., Faber S. M., González J. J., 1992, *ApJ*, 398, 69
- Worthey G., Faber S. M., González J. J., Burnstein D., 1994, *ApJS*, 94, 687
- Worthey G., Dorman B., Jones L. A., 1996, *AJ*, 112, 948

This paper has been typeset from a $\text{\TeX}/\text{\LaTeX}$ file prepared by the author.